ARTICLE

Robust Superhydrophobic Mats based on Electrospun Crystalline Nanofibers Combined with a Silane Precursor

Song Hee Park,[†] Song Min Lee,[†] Ho Sun Lim,[‡] Joong Tark Han,[§] Dong Ryeol Lee,[||] Hwa Sung Shin,[⊥] Youngjin Jeong,*[,†] Jooyong Kim,*[,†] and Jeong Ho Cho*[,†]

Department of Organic Materials and Fiber Engineering, Soongsil University, Seoul 156-743, Korea, Department of Materials Science and Engineering, Institute for Soldier Nanotechnologies, Massachusetts Institute of Technology, Cambridge, Massachusetts 02139, Nano Carbon Materials Research Team, Korea Electrotechnology Research Institute, Changwon, 641-120, Korea, Department of Physics, Soongsil University, Seoul 156-743, Korea, and Department of Biological Engineering, Inha University, Incheon 402-751, Korea

ABSTRACT We demonstrate the fabrication of solvent-resistant, mechanically robust, superhydrophobic nanofibrous mats by electrospinning of poly(vinylidene fluoride) (PVDF) in the presence of inorganic silane materials. The solvent resistance and mechanical strength of nanofibrous mats were dramatically increased through the crystallization of as-spun PVDF fibers or incorporation of a tetraethyl orthosilicate (TEOS) sol into the nanofibrous matrix. The electrospun nanofibrous mats yielded a water contact angle of 156° that did not vary with TEOS content. The solvent resistance and mechanical robustness of the electrospun mats were significantly enhanced through extensive cross-linking of TEOS, even after short PVDF annealing times. The interpenetrating polymer network, which embeds polymer chains in a TEOS network, allows the fabrication of robust functional nanofibers by combining semicrystalline polymers with electrospinning techniques.

KEYWORDS: electrospun nanofibers • superhydrophobic • poly(vinylidene fluoride) • tetraethyl orthosilicate • solvent resistance • mechanical strength

INTRODUCTION

The textured hierarchical surface structures of lotus leaves endow them with a surprising ability to resist droplet adhesion, allowing their surfaces to self-clean as the droplets glide across the leaves (1). Such superhydrophobic surfaces, with water contact angles (CAs) greater than 150°, have been intensively studied in basic research, as well as for practical applications such as microfluidics, textiles, and automobiles (2). Superhydrophobic surfaces have been achieved through the control of both the chemical composition and morphological structures present on a surface (3). To date, many fabrication methods have produced superhydrophobic surfaces, including chemical deposition, layer-by-layer deposition, colloidal assembly, and lithographic or template-based techniques (4). However, because these sophisticated fabrication processes are time-consuming, expensive, and complicated, practical applications of these methods are restricted. Moreover, practical applications of superhydrophobic surfaces require robust environmental stability with respect to solvent resistance and mechanical abrasion.

Electrospinning is an efficient and simple tool for the fabrication of continuous polymeric nanofibrous nanostructured substrates with a high surface roughness resulting from a high surface-to-volume ratio (5). Electrospun fibers find applications in filtration technologies, tissue engineering, optical devices, and sensors (6). Electrospun nanofibers are produced by applying an electrical bias from the tip of a syringe, filled with polymer solution, to a grounded collection plate. The texture of the electrospun nanofibers can be easily tuned from bead-like to fibrous by controlling the viscosity and molecular weight of the polymer solution and applied voltage (3c, 6). Thus, electrospinning is a versatile and promising route to developing superhydrophobic surfaces from polymers that feature low surface energies.

Several types of superhydrophobic surfaces, produced by electrospinning techniques, have been described recently (6, 7). Superhydrophobic polystyrene electrospun mats were produced by controlling the polymer solution properties and electrospinning conditions (7d). The water CAs of these polystyrene mats could be varied from 160° to 140° by tuning the surface morphology from bead-like to fibrous. Fiber morphological changes were also used to tune the hydrophobic behavior of polyacrylonitrile fiber electrospun mats (6b). Superhydrophobic poly(caprolactone) electrospun mats were prepared by coating polymer fibers with a thin

* To whom correspondence should be addressed. Tel: +82-2-820-0995. Fax: +82-2-817-8346. E-mail: jhcho94@ssu.ac.kr (J.H.C.); jykim@ssu.ac.kr (J.K.); yjeong@ssu.ac.kr (Y.J.).

Received for review September 26, 2009 and accepted February 15, 2010

[†] Department of Organic Materials and Fiber Engineering, Soongsil University.

[‡] Institute for Soldier Nanotechnologies, Massachusetts Institute of Technology.

[§] Nano Carbon Materials Research Team, Korea Electrotechnology Research Institute.

[||] Department of Physics, Soongsil University.

[⊥] Department of Biological Engineering, Inha University.

DOI: 10.1021/am100005x

Published on Web 02/26/2010

layer of perfluoroalkyl methacrylate that was polymerized by initiated chemical vapor deposition. Perfluoroalkyl methacrylate, which has an extremely low surface free energy and has been used in surface coatings, yielded a stable superhydrophobic surface with a water CA of 175° and a sliding angle of less than 2.5° (7e). However, the solvent resistance and mechanical strength of these superhydrophobic nanofibrous webs, which are important factors for practical applications, have not been extensively investigated.

In this paper, we introduce a facile method for improving the solvent resistance and mechanical stability of superhydrophobic nanofibrous mats for use in structural material coating applications. To produce such robust superhydrophobic surfaces, we combine two material preparation techniques: (i) the crystallinity of the semicrystalline polymer, poly(vinylidene fluoride) (PVDF), is tightly controlled by thermal annealing, and (ii) structural reinforcement is conferred by the cross-linking of a silane precursor, tetraethyl orthosilicate (TEOS). PVDF is an excellent material for membrane applications because of its easy processing, high strength, and good resistance to solvents, acids, and bases (8). Incorporation of TEOS improves the solvent resistance and mechanical robustness of the nanofibers because of the formation of a siloxane network interspersed among the PVDF chains, which shortens the annealing time required for PVDF crystallization. The mechanical robustness of the electrospun mats was investigated by friction tests, which measured the frictional force produced by the nanofibrous mat's resistance to deformation under abrasion. The interpenetrating polymer network allows the fabrication of robust nanofibrous structures by combining semicrystalline polymers with electrospinning techniques.

EXPERIMENTAL SECTION

Materials and Sample Preparation. Poly(vinylidene fluoride) (PVDF) was purchased from Solvay Solexis (Belgium). Tetraethyl orthosilicate (TEOS), *N*,*N*-dimethylformamide (DMF), and acetone were purchased from Sigma-Aldrich (USA). A 20 wt % PVDF solution was prepared by dissolving PVDF in a mixture of DMF and acetone (DMF/acetone = 2:1, volume ratio) with stirring for 12 h at 50 °C. Subsequently, TEOS was added to the solution to yield mass ratios of 0%, 30%, or 50% TEOS relative to that of PVDF (PVDF-TEOS0%, PVDF-TEOS30%, and PVDF-TEOS50%, respectively), and the solutions were stirred at 50 °C for 4 h. The polymer solutions were electrospun into fibrous webs using an electrospinning system equipped with a power supply. A voltage of 16 kV was applied across a fixed collection distance of 15 cm between the tip of the needle (diameter 0.61 mm) and the grounded aluminum foil. Nanofibers were spun over the course of 2 h, resulting ~20 × 20 cm^2 mats. The electrospun PVDF and PVDF/TEOS hybrid electrospun mats were annealed at 100 °C for varying lengths of time (20, 40, 80, 90, and 120 min).

Characterization. The morphologies of the electrospun PVDF nanofibrous mats were imaged by scanning electron microscopy (JEOLJSM-6360). X-ray diffraction (XRD) patterns were collected under CuKα radiation (λ = 1.54 Å) using a Rigaku X-ray diffraction spectrometer equipped with an area detector. Fourier transform infrared (FT-IR) spectra were recorded on an FTIR-6300 (JASCO) spectrometer in transmittance mode with a resolution of 4 cm^{-1}. Angle-resolved X-ray photoelectron spectroscopy (XPS) was performed at the 4B1 beamline at the Pohang Accelerator Laboratory. Emission angles were varied from 90° to 30°. Three samples obtained in different batches were used for XRD, FT-IR, and XPS measurements to minimize the experimental error. Water contact angle (CA) measurements were conducted with a drop shape analysis system (Krüss). The relative changes in frictional properties of electrospun nanofibrous mats were characterized on a home-built friction test machine. To exclude the error induced by the testing conditions, more than five samples in three different batches were used.

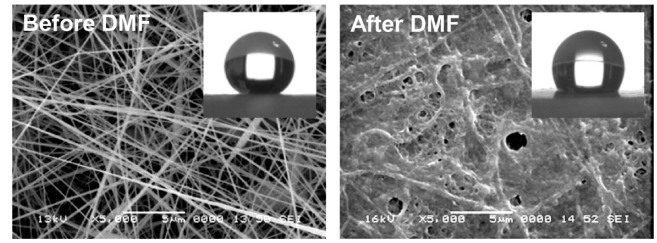

FIGURE 1. SEM images and contact angles of the electrospun poly(vinylidene fluoride) (PVDF) nanofibrous mats before and after exposure to DMF.

RESULTS AND DISCUSSION

Figure 1 shows SEM images of electrospun pristine PVDF-TEOS0% nanofibrous mats without thermal annealing. The average diameter of each fiber was around 150 nm. The water CA of the PVDF nanofibrous mat was measured to be 155.5°, which indicated superhydrophobicity. In particular, the PVDF mat showed gecko-state superhydrophobicity, which is not only superhydrophobic but also strongly adhesive to water. The water droplet does not easily slide even when the PVDF nanofibrous mats were tilted vertically or turned upside down. This high water-adhesive behavior arose from a large van der Waals force between the nanofibrous structures of the PVDF mats and water. After exposure to DMF (by dropping 1 mL onto the fiber mat), the nanofiber structure collapsed because of the low crystallinity of PVDF, yielding a surface water CA of 121.5° (Figure 1).

To enhance the fibrous structure's solvent (DMF) resistance, solutions containing either PVDF or either of the two PVDF/TEOS mixtures were electrospun into fibrous mats, followed by thermal annealing at 100 °C. The average diameter of the electrospun fibers produced by the PVDF/TEOS admixtures were comparable to the fiber diameters of pristine PVDF, as shown in Figure 2a, because the viscosities of the electrospun solutions were similar (6b, 7e).

Figure 2b shows the SEM images of PVDF and PVDF/TEOS hybrid electrospun mats, annealed at 100 °C for varying lengths of time and then exposed to DMF. The pristine PVDF nanofibrous mats (without TEOS) were thoroughly damaged if the mats had not been subjected to thermal annealing. For annealing times below 80 min, DMF partially damaged the fibrous structures. However, after 90 min annealing, the PVDF fibrous structures did not conglomerate under DMF exposure. Notably, the PVDF-TEOS50% nanofibrous mat was stable in DMF, even after only 40 min thermal annealing, whereas the structural integrity, under DMF exposure, of the pristine PVDF nanofiber was only obtained after a minimum of 90 min thermal annealing. The addition of TEOS to the electrospun nanofibers shortened

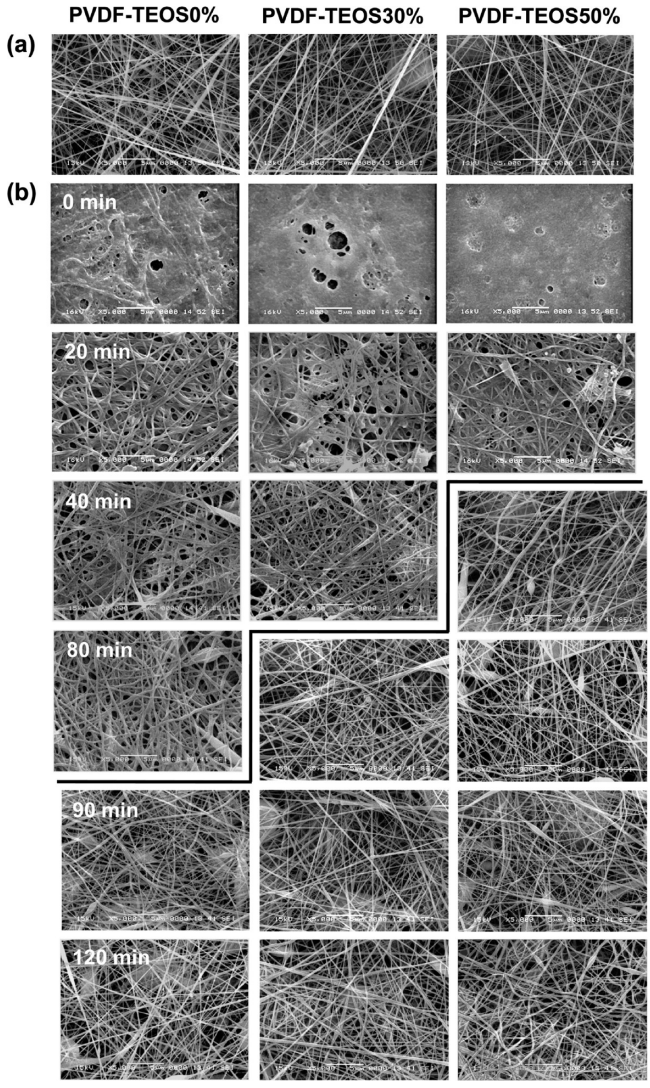

FIGURE 2. SEM images of (a) as-spun and (b) thermally annealed (at 100 °C for 0−120 min, as indicated) electrospun PVDF-TEOS0%, PVDF-TEOS30%, and PVDF-TEOS50% after exposure to DMF.

the annealing time required to preserve the fibrous structure's morphology under DMF exposure. Note that the structural integrity of PVDF-TEOS50% nanofiber under two different solvents such as dimethylacetamide (DMAc) and dimethylsulfoxide (DMSO) was also obtained after only 40 min thermal annealing (Figure S1, Supporting Infromation).

The chemical and physical properties of the PVDF nanofibrous mats, with thermal annealing, were investigated by XRD and FT-IR spectroscopy. Figure 3a shows the XRD patterns of PVDF-TEOS0% mats submitted to various annealing times. The diffraction peaks at $2\theta = 17.8°$, 18.4°, 20.0°, 26.5°, 36.3°, and 38.6° corresponded to the (100), (020), (110), (021), (200), and (002) α-phase reflections, respectively. Distinct β diffraction peak also appeared at $2\theta = 20.7°$, which corresponded to (110)(200) reflection. These peak positions agreed well with the values reported in the literature (9). The XRD patterns indicated the coexistence of α and β phases in the electrospun PVDF nanofibers, with the α-type crystal structure present to a larger extent. The intensities of both α and β phase diffraction peaks increased for longer annealing times.

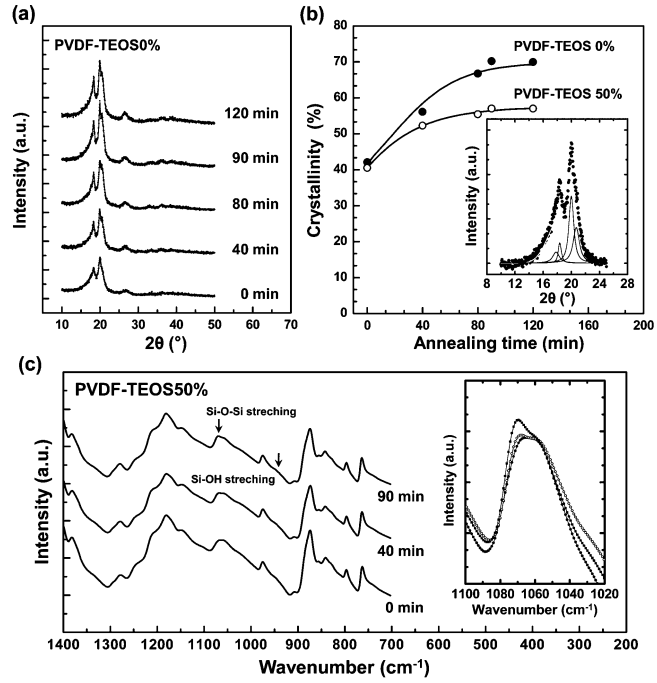

FIGURE 3. (a) XRD patterns of electrospun PVDF-TEOS0% nanofibrous mats submitted to various annealing times. (b) Total crystallinity of PVDF-TEOS0% and PVDF-TEOS50% nanofibrous mats at different annealing times. The inset shows the XRD peaks of PVDF-TEOS0% nanofibrous mats without annealing. (c) FT-IR spectra of electrospun PVDF-TEOS50% nanofibrous mats submitted to various annealing times. The inset shows the magnified spectra in the region of Si−O−Si stretching: (●, 0 min; ○, 40 min; □, 90 min).

The degree of crystallinity was calculated from the ratio of the area corresponding to crystalline parts (dark gray) to the total area (crystalline and amorphous parts, light gray) (9a). The inset of Figure 3 (b) shows representative XRD peaks for the PVDF-TEOS0% nanofibrous mats without annealing. The total crystallinity of PVDF-TEOS0% and PVDF-TEOS50% nanofibrous mats, annealed for various lengths of time, are presented in Figure 3b. The total crystallinity increased for both PVDF-TEOS0% and PVDF-TEOS50% nanofibrous mats with increasing annealing time. The crystallinity of PVDF-TEOS0% saturated at 70% after annealing at 100 °C for 90 min. It was apparent from the SEM images shown in Figure 2b that the solvent (DMF) resistance of PVDF-TEOS0% was obtained only for crystallinities above 70%. The total crystallinity of PVDF-TEOS50% nanofibers saturated at 52%, after 40 min of thermal annealing, indicating that the addition of TEOS disturbed the crystallization of PVDF. Despite the lower degree of crystallinity, PVDF-TEOS50% nanofibers displayed solvent (DMF) resistance after a much shorter annealing time of 40 min. The hybridized PVDF-TEOS structure, therefore, dramatically enhanced the solvent resistance of the nanofiber, despite low crystallinity.

The FT-IR spectra for PVDF-TEOS 50% nanofibrous mats, submitted to various annealing times, were measured to investigate the chemical origin of the solvent (DMF) resistance conferred by TEOS, Figure 3c. The FT-IR spectrum of PVDF was characterized by distinctive bands at 764, 796, and 976 cm^{-1}, corresponding to the α-phase, and at 842 and 1279 cm^{-1}, corresponding to the β-phase (10). The peak at

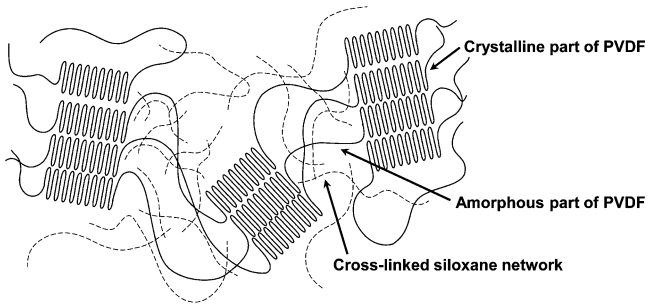

FIGURE 4. Schematic of the cross-linking of TEOS among PVDF chains.

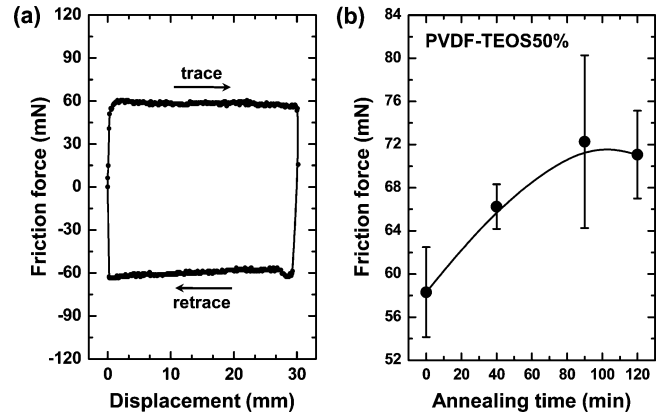

FIGURE 5. (a) Representative frictional force loop for PVDF-TEOS50% nanofibrous mats without annealing. (b) Frictional force versus annealing time for PVDF-TEOS50% nanofibrous mats.

~1070 cm^{-1} was ascribed to Si−O−Si stretching vibrations. The shoulder-like peaks at ~945 cm^{-1} were attributed to Si−OH groups (11). For longer annealing times, the relative intensity of the Si−O−Si peak increased and shifted to higher wavenumbers, as shown in the inset of Figure 3c. On the other hand, the peak corresponding to the Si−OH stretches gradually decreased. The IR spectral changes indicated that, during annealing, the siloxane network grew by condensation between silanol groups (11d).

The chemical changes observed in the FT-IR spectra can be explained by the formation of a siloxane network interspersed among the PVDF chains. During the preparation of the PVDF/TEOS solution, prior to electrospinning, water present in the DMF solvent partially hydrolyzed TEOS to form silanol groups. Condensation reactions among the silanol groups produced low molecular weight polymers. When the electrospun nanofibers were annealed at 100 °C under ambient conditions, the condensation reaction was accelerated, forming a cross-linked silica network that embedded the PVDF chains within the TEOS network, as shown in Figure 4. From thermogravimetric analysis (TGA) as shown in Figure S2, Supporting Information, the amount of the siloxane network in PVDF/TEOS hybrid electrospun mats was found to be 5.1 and 7.9% for PVDF-TEOS30%, and PVDF-TEOS50%, respectively. Furthermore, PVDF/TEOS hybrid nanofibrous mats show the better thermal stability compared to pristine PVDF mats.

Table 1 summarizes the CAs of spin-coated and electrospun PVDF-TEOS0%, PVDF-TEOS30%, and PVDF-TEOS50% nanofibrous mats, prepared with annealing for various lengths of time. The measured CA of the spin-coated PVDF-TEOS0% film was 125.1°, much lower than the superhydrophobic CA, 155.5°, of fibrous form of PVDF-TEOS0%. The measured water CAs were independent of both annealing time and TEOS content, suggesting that PVDF chains preferentially partitioned toward the hybrid polymer surface to lower the overall nanofiber surface energy (12). To determine the surface chemical composition of the PVDF-TEOS nanofibers, angle-resolved XPS measurements were performed on the spin-coated PVDF-TEOS50% film, as shown in Figure S3, Supporting Information. As the emission angle was reduced from 90° to 30°, the F_{1s} peak intensity from PVDF increased, and the Si_{1s} peak intensity from TEOS simultaneously decreased. This result indicated that the topmost layers of the hybrid nanofiber structures were enriched with PVDF such that the water CAs were independent of the TEOS content. Therefore, robust superhydrophobic nanofibrous mats were successfully obtained by the cross-linking of TEOS without altering the water CA. The electrospun PVDF mats with bead-on-string structures may have significantly larger CAs because of the fibers' multiscale hierarchical morphology.

The improved surface mechanical strength of electrospun PVDF nanofibrous mats was quantified by measuring the friction properties of the mats by means of a home-built apparatus. The nanofibrous mats were loaded under a constant applied force of 10 g; the applied load was moved relative to the surface while maintaining the 10 g load, and the friction experienced during 30 mm trace−retrace cycle at 1 mm/s was recorded (Figure 5a). The probe contacting the nanofibrous mats consisted of a stainless steel mass with a contact area of 50 mm^2, length of 10 mm, and width of 5 mm. Figure 5b shows the measured frictional force as a function of annealing times for the PVDF-TEOS50% nanofibrous mats. At longer annealing times, the frictional force increased considerably. The frictional force increased by 20% for more extensive TEOS cross-linking. The frictional force produced by the PVDF nanofibrous mats arose mainly from resistance to deformation because the surface properties of all PVDF nanofibrous mats were similar, as shown in

Table 1. Water Contact Angles of Spin-Coated and Electrospun PVDF-TEOS0%, PVDF-TEOS30%, and PVDF-TEOS50% at Different Annealing Times

	PVDF-TEOS0%		PVDF-TEOS30%		PVDF-TEOS50%	
	spin-coated	electrospun	spin-coated	electrospun	spin-coated	electrospun
0 min	125.1°	155.5°	130.1°	156.2°	126.3°	157.4°
80 min	123.8°	156.2°	127.7°	156.5°	127.3°	155.7°
120 min	123.5°	155.8°	128.3°	157.1°	126.7°	156.2°

Table 1. The PVDF-TEOS50% nanofibrous mat, produced without annealing, deformed easily, providing less deformation resistance to the probe and yielding a low measured frictional force. Longer annealing times, which permitted more extensive condensation and cross-linking of the TEOS, presumably created a more extensive network throughout the nanofiber structure, increasing the deformation resistance of each nanofiber in the mats. The high deformation resistance resulted in a high surface mechanical strength. In contrast, the frictional force of the PVDF-TEOS0% fibrous mats slightly increased within the error range with annealing time, which indicates that the cross-linking of the TEOS is more dominant than the crystallinity of PVDF in the surface mechanical properties of PVDF nanofibrous mats.

CONCLUSION

We report a simple method for fabricating structurally robust and solvent resistant superhydrophobic nanofibrous mats by electrospinning PVDF in the presence of TEOS. Thermal annealing at 100 °C increased the PVDF crystallinity and simultaneously allowed the formation of an extensively cross-linked TEOS structural network embedded among the PVDF chains. The increase in PVDF crystallinity, produced by annealing for 90 min, resulted in strong solvent (DMF) resistance of the electrospun PVDF fibrous webs. Interestingly, although TEOS inhibited the crystallization of PVDF (a crystallinity of only 53% was achievable for PVDF-TEOS50% compared to 70% for the PVDF-TEOS0% nanofibrous mats), solvent resistance of PVDF-TEOS50% was obtained for much shorter annealing times, presumably by means of the structural reinforcement conferred by the siloxane network. The hydrophobicity of the nanofibrous mats was independent of TEOS content, and all electrospun fiber samples yielded water CAs of around 156°. Mechanical strength dramatically increased with the extent of TEOS cross-linking, as measured by the nanofibrous mats' resistance to deformation. Solvent resistant and mechanically robust superhydrophobic nanofibrous mats, fabricated via optimized PVDF crystallization and TEOS cross-linking, may be suitable for use in semicrystalline polymer technologies and engineering plastics applications.

Acknowledgment. The authors thank Soongsil University Research Fund for their financial support and the Pohang Accelerator Laboratory for providing the 4B1 and 5A beamline used in this study.

Supporting Information Available: SEM images of as-spun and thermally annealed (at 100 °C for 40 min) electrospun PVDF-TEOS50% nanofibrous mats after exposure to (a) DMAc and (b) DMSO (Figure S1), weight loss (%) as function of the temperature of the PVDF/TEOS nanofiber mats measured by thermogravimetric analysis (TGA) (Figure S2), and F_{1s} and Si_{2p} core level angle-resolved XPS spectra of the spin-coated PVDF-TEOS50% film (Figure S3). This material is available free of charge via the Internet at http://pubs.acs.org.

REFERENCES AND NOTES

(1) (a) Sun, T. L.; Feng, L.; Gao, X. F.; Jiang, L. *Acc. Chem. Res.* **2005**, *38*, 644. (b) Barthlott, W.; Neinhuis, C. *Planta* **1997**, *202*, 1.

(2) (a) Azad, A. M.; Matthews, T.; Swary, J. *Mater. Sci. Eng. B.* **2005**, *123*, 252. (b) Dror, Y.; Salalha, W.; Avrahami, R.; Zussman, E.; Yarin, A. L.; Dersch, R.; Greiner, A.; Wendorff, J. H. *Small* **2007**, *6*, 1064. (c) Gibson, P. W.; Shreuder-Gibson, H. L.; Rivin, D. *AIChE J.* **1999**, *45*, 190. (d) Wang, X. Y.; Drew, C.; Lee, S. H.; Senecal, K. J.; Kumar, J.; Samuelson, L. A. *Nano Lett.* **2002**, *2*, 1273.

(3) (a) Callies, M.; uéré, D. *Soft Matter* **2005**, *1*, 55. (b) Li, X.-M.; Reinhoudt, D.; C.-Calama, M. *Chem. Soc. Rev.* **2007**, *36*, 1350. (c) Li, D.; Xia, Y. *Adv. Mater.* **2004**, *16*, 1151. (d) Han, J. T.; Lee, D. H.; Ryu, C. Y.; Cho, K. *J. Am. Chem. Soc.* **2004**, *126*, 4796. (e) Han, J. T.; Zheng, Y.; Cho, J. H.; Xu, X.; Cho, K. *J. Phys. Chem. B* **2005**, *109*, 20773.

(4) (a) He, B.; Patankar, N. A.; Lee, J. *Langmuir* **2003**, *19*, 4999. (b) Extrand, C. W. *Langmuir* **2002**, *18*, 7991. (c) Teshima, K.; Sugimura, H.; Inoue, Y.; Takai, O.; Takano, A. *Langmuir* **2003**, *19*, 10624. (d) Li, H.; Wang, X.; Song, Y.; Liu, Y.; Li, Q.; Jiang, L.; Zhu, D. *Angew. Chem., Int. Ed.* **2001**, *40*, 1743. (e) Yan, H.; Kurogi, K.; Mayama, H.; Tsujii, K. *Angew. Chem., Int. Ed.* **2005**, *44*, 3453. (f) Shiu, J. Y.; Kuo, C. W.; Chen, P. L.; Mou, C. Y. *Chem. Mater.* **2004**, *16*, 561.

(5) (a) Li, D.; Xia, Y. *Nano Lett.* **2003**, *4*, 933. (b) Huang, Z.; Zhang, Y.; Kotaki, M.; Ramakrishna, S. *Compos. Sci. Technol.* **2003**, *63*, 2223. (c) Teo, W. E.; Ramakrishna, S. *Nanotechnol.* **2006**, *17*, R89. (d) Greiner, A.; Wendorff, J. H. *Angew. Chem., Int. Ed.* **2007**, *46*, 5670. (e) Subbiah, T.; Bhat, G. S.; Tock, R. W.; Parameswaran, S.; Ramkumar, S. S. *J. Appl. Polym. Sci.* **2005**, *96*, 557. (f) Sigmund, W.; Yuh, J.; Park, H.; Maneeratana, V.; Pyrgiotakis, G.; Daga, A.; Taylor, J.; Nino, J. C. *J. Am. Ceram. Soc.* **2006**, *89*, 395. (g) Li, W.-J.; Mauck, R. L.; Tuan, R. S. *J. Biomed. Nanotechnol.* **2005**, *1*, 259. (h) Raagavan, N. N. V.; Karnan, P.; Jagadeeswaran, S. *Synth. Fibers* **2005**, *34*, 16.

(6) (a) Tuteja, A.; Choi, W.; Mabry, J. M.; McKinley, G. H.; Cohen, R. E. *Proc. Natl. Acad. Sci.* **2008**, *105*, 18200. (b) Acatay, K.; Simsek, E.; Ow-Yang, C.; Menceloglu, Y. Z. *Angew. Chem., Int. Ed.* **2004**, *116*, 5322.

(7) (a) Bergshoef, M. M.; Vancso, G. J. *Adv. Mater.* **1999**, *11*, 1362. (b) Ma, M.; Gupta, M.; Li, Z.; Zhai, L.; Gleason, K. K.; Cohen, R. E.; Rubner, M. F.; Rutledge, G. C. *Adv. Mater.* **2007**, *19*, 255. (c) Ogawa, T.; Ding, B.; Sone, Y.; Shiratori, S. *Nanotechnology* **2007**, *18*, 165607. (d) Jiang, L.; Zhao, Y.; Zhai, J. *Angew. Chem., Int. Ed.* **2004**, *43*, 4338. (e) Ma, M.; Mao, Y.; Gupta, M.; Gleason, K. K.; Rutledge, G. C. *Macromolecules* **2005**, *38*, 9742.

(8) (a) Chen, Y.; Kim, H. *Appl. Surf. Sci.* **2009**, *255*, 7073. (b) Shah, D.; Maiti, P.; Gunn, E.; Schmidt, D. F.; Jiang, D. D.; Batt, C. A.; Giannelis, E. P. *Adv. Mater.* **2004**, *16*, 1173.

(9) (a) Du, C.; Zhu, B.-K.; Xu, Y.-Y. *J. Appl. Polym. Sci.* **2007**, *104*, 2254. (b) Nasir, M.; Matsumoto, H.; Danno, T.; Minagawa, M.; Irisawa, T.; Shioya, M.; Tanioka, A. *J. Polym. Sci., Part B* **2006**, *44*, 779.

(10) (a) Yee, W. A.; Kotaki, M.; Liu, Y.; Lu, X. *Polymer* **2007**, *48*, 512. (b) Yoon, S.; Prabu, A.; Kim, K. J.; Park, C. *Macromol. Rapid Commun.* **2008**, *29*, 1316.

(11) (a) Karmaker, B.; Ganguli, G. *J. Mater. Chem.* **2000**, *10*, 2289. (b) Zhang, X.; Wu, Y.; He, S.; Yang, D. *Surf. Coat. Technol.* **2007**, *201*, 6051. (c) Stefanescu, M.; Stoia, M.; Stefanescu, O. *J. Sol–Gel Technol.* **2007**, *41*, 71. (d) Zhang, Z. *Langmuir* **1997**, *13*, 473.

(12) Iyengar, D. R.; Perutz, S. M.; Dai, C.-A.; Ober, C. K.; Kramer, E. J. *Macromolecules* **1996**, *29*, 1229.

AM100005X